

# Coherent radiation by magnets with exchange interactions

V.I. Yukalov<sup>1,\*</sup> and E.P. Yukalova<sup>2</sup>

<sup>1</sup>*Bogolubov Laboratory of Theoretical Physics,  
Joint Institute for Nuclear Research, Dubna 141980, Russia*

<sup>2</sup>*Laboratory of Information Technologies,  
Joint Institute for Nuclear Research, Dubna 141980, Russia*

## Abstract

A wide class of materials acquires magnetic properties due to particle interactions through exchange forces. These can be atoms and molecules composing the system itself, as in the case of numerous magnetic substances. Or these could be different defects, as in the case of graphene, graphite, carbon nanotubes, and related materials. The theory is suggested describing fast magnetization reversal in magnetic systems, whose magnetism is caused by exchange interactions. The effect is based on the coupling of a magnetic sample with an electric circuit producing a feedback magnetic field. This method can find various applications in spintronics. The magnetization reversal can be self-organized, producing spin superradiance. A part of radiation is absorbed by a resonator magnetic coil. But an essential part of radiation can also be emitted through the coil sides.

**Keywords:** Magnetic materials, Exchange interactions, Magnetic graphene, Spintronics, Spin superradiance, Maser radiation

**PACS numbers:** 84.40.Dc; 84.40.Ik; 84.90+a; 85.75.Hh; 85.75.Ff

\*Corresponding author: V.I. Yukalov

**E-mail:** yukalov@theor.jinr.ru

# 1 Introduction

Magnetic materials, whose magnetism is caused by exchange interactions, form a very wide class of magnets of different sizes, including the samples of nanosizes, which find a variety of applications [1]. A novel class of exchange-interaction magnetic materials is the graphene family with defects, including graphene flakes and ribbons, graphite, and carbon nanotubes [2–4]. Magnetic materials find numerous applications in quantum electronics, for example, in spintronics, information processing etc.

In the present paper, we concentrate on two interconnected features of magnetic materials: (i) First, we study the way of fast magnetization reversal in these materials that is a property crucially important for spintronics and information processing. We show that by coupling a magnetic sample to a resonant electric circuit it is possible to achieve fast magnetization reversal. The details of the reversal can be easily regulated by varying the system parameters. (ii) Second, fast magnetization reversal should produce magneto-dipole spin radiation in radio-frequency or microwave region. However, a large part of this radiation would be absorbed by the coil of the coupled electric circuit. We aim at studying whether some part of the maser radiation could be emitted through the coil sides. The possibility of this effect would essentially widen the region of applicability of such magnetic materials.

The fact that coupling a resonant electric circuit to a spin system could essentially influence spin dynamics is the essence of the Purcell effect [5]. A detailed theory of spin dynamics, employing the Purcell effect, has been developed for nuclear spins [6–10], magnetic nanomolecules [11–13], and magnetic nanoclusters [14–17] (see also the review article [18]). The characteristic feature of all these materials is that their particle interactions are described by dipolar forces. Also, only the total radiation intensity has been considered. However, in the typical setup, the magnetic sample is inserted into a coil of a resonant magnetic circuit, so that an essential part of radiation is absorbed by this coil. In order to understand whether some part of magneto-dipole radiation could be emitted through the coil sides, it is necessary to study the spatial distribution of the radiation.

The main novelty of the present paper is twofold: (i) We consider the class of magnetic materials with exchange interactions. This class is widespread and important, including a number of known magnetic materials as well as new nanomaterials, such as graphene with defects. (ii) We study the spatial distribution of radiation in order to conclude whether a sample inside a coil could serve as an emitter of radiation passing through the coil sides.

## 2 Magnets with exchange interactions

The Hamiltonian of a system of  $N$  particles is the sum

$$\hat{H} = \hat{H}_{ex} - \mu_0 \sum_{j=1}^N \mathbf{B} \cdot \mathbf{S}_j . \quad (1)$$

The first term is the Hamiltonian of an anisotropic Heisenberg model,

$$\hat{H}_{ex} = - \frac{1}{2} \sum_{i \neq j} [J_{ij} (S_i^x S_j^x + S_i^y S_j^y) + I_{ij} S_i^z S_j^z] , \quad (2)$$

describing particles with exchange interactions. The second is a Zeeman term, with  $\mu_0$  being magnetic moment, and with the total magnetic field

$$\mathbf{B} = B_0 \mathbf{e}_z + H \mathbf{e}_x \quad (3)$$

consisting of an external magnetic field  $B_0$  along the  $z$  axis and a feedback field  $H$ , along the  $x$  axis, caused by the magnetic coil of an electric circuit. The sample is inserted into the coil, with its axis along the  $x$  axis. The feedback field is defined by the Kirchhoff equation that can be written [8,9,18] as

$$\frac{dH}{dt} + 2\gamma H + \omega^2 \int_0^t H(t') dt' = -4\pi \frac{dm_x}{dt} . \quad (4)$$

Here  $\gamma$  is the circuit attenuation,  $\omega$  is the circuit natural frequency, and the effective electromotive force is due to the moving magnetization of the sample,

$$m_x = \frac{\mu_0}{V_c} \sum_{j=1}^N \langle S_j^x \rangle , \quad (5)$$

where  $V_c$  is the coil volume and angle brackets imply statistical averaging.

The  $z$  axis is assumed to be the axis of the easy magnetization, so that  $I_{ij}$  should be larger than  $J_{ij}$ . If exchange interactions are due to electrons, then  $\mu_0 < 0$ . Therefore, if  $B_0 > 0$ , then the equilibrium spin value  $S_0$  of a particle is negative,  $S_0 < 0$ . In this case, the Zeeman frequency is positive,

$$\omega_0 \equiv -\mu_0 B_0 > 0 . \quad (6)$$

The effective particle spin  $S$  can be arbitrary. The ladder spin operators

$$S_j^\pm \equiv S_j^x \pm i S_j^y$$

satisfy the commutation relations

$$[S_i^+, S_j^-] = 2\delta_{ij} S_j^z , \quad [S_i^-, S_j^z] = 2\delta_{ij} S_j^- .$$

In terms of the ladder spin operators, the exchange Hamiltonian (2) is

$$\hat{H}_{ex} = -\frac{1}{2} \sum_{i \neq j} (J_{ij} S_i^+ S_j^- + I_{ij} S_i^z S_j^z) . \quad (7)$$

Writing down the Heisenberg equations of motion, we compliment them by the attenuation  $\gamma_1$ , caused by spin-lattice interactions and  $\gamma_2$ , due to other spin interactions, e.g., dipole interactions that usually are smaller than the exchange interactions. In that way, the equations of motion read as

$$i \frac{dS_j^\pm}{dt} = [S_j^\pm, \hat{H}] - i\gamma_2 S_j^\pm , \quad i \frac{dS_j^z}{dt} = [S_j^z, \hat{H}] - i\gamma_1 (S_j^z - S_0) . \quad (8)$$

Accomplishing the related commutations, we get the equations for the transverse spin,

$$\frac{dS_i^-}{dt} = i \sum_{j(\neq i)} (I_{ij} S_i^- S_j^z - J_{ij} S_i^z S_j^-) - i\omega_0 S_i^- - i\mu_0 H S_i^z - \gamma_2 S_i^- , \quad (9)$$

and for the longitudinal spin

$$\frac{dS_i^z}{dt} = \frac{i}{2} \sum_{j(\neq i)} J_{ij} (S_i^+ S_j^- - S_i^- S_j^+) + \frac{i}{2} \mu_0 H (S_i^+ - S_i^-) - \gamma_1 (S_i^z - S_0) . \quad (10)$$

### 3 Stochastic mean-field approximation

We shall be interested in the evolution of the averaged quantities characterizing the *transition function*

$$u \equiv \frac{1}{NS} \sum_{j=1}^N \langle S_j^- \rangle , \quad (11)$$

the *coherence intensity*

$$w \equiv \frac{1}{N(N-1)S^2} \sum_{i \neq j}^N \langle S_i^+ S_j^- \rangle , \quad (12)$$

and the *spin polarization*

$$z \equiv \frac{1}{NS} \sum_{j=1}^N \langle S_j^z \rangle . \quad (13)$$

Averaging equations (9) and (10), we invoke *stochastic mean-field approximation* [19], replacing spin pair correlators as

$$\langle S_i^\alpha S_j^\beta \rangle \rightarrow \langle S_i^\alpha \rangle \langle S_j^\beta \rangle + \langle S_i^\alpha \rangle \delta S_j^\beta + \langle S_j^\beta \rangle \delta S_i^\alpha , \quad (14)$$

where  $i \neq j$  and  $\delta S_j^\alpha$  is treated as a stochastic variable, such that its stochastic average be zero:

$$\langle \langle \delta S_j^\alpha \rangle \rangle = 0 . \quad (15)$$

Then the averages  $\langle S_j^\alpha \rangle$  become functions of the stochastic variables.

Also, we introduce the composite stochastic variables

$$\begin{aligned} \xi_0 &\equiv \sum_{j(\neq i)} (J_{ij} \delta S_i^z - I_{ij} \delta S_j^z) , & \xi &\equiv \sum_{j(\neq i)} (I_{ij} \delta S_i^- - J_{ij} \delta S_j^-) , \\ \varphi &\equiv \sum_{j(\neq i)} J_{ij} (\delta S_i^- - \delta S_j^-) . \end{aligned} \quad (16)$$

And we define the effective anisotropy

$$\Delta J \equiv \frac{1}{N} \sum_{i \neq j} (I_{ij} - J_{ij}) . \quad (17)$$

We assume that  $\langle S_j^\alpha \rangle$  does not depend on the index enumerating spins and that the variables (16) also are not index-dependent.

In this way, from equation (9), we obtain the equation for the transition function,

$$\frac{du}{dt} = -i(\omega_0 + \xi_0 - S\Delta Jz - i\gamma_2)u - i(\mu_0 H - \xi)z , \quad (18)$$

and for the coherence intensity,

$$\frac{dw}{dt} = -2\gamma_2 w + i(\mu_0 H - \xi^*)zu - i(\mu_0 H - \xi)zu^* . \quad (19)$$

While equation (10) yields the equation for the spin polarization,

$$\frac{dz}{dt} = \frac{i}{2} u^* (\mu_0 H - \varphi) - \frac{i}{2} u (\mu_0 H - \varphi^*) - \gamma_1 (z - \zeta), \quad (20)$$

where  $\zeta \equiv S_0/S$ . The initial conditions

$$u_0 = u(0), \quad w_0 = w(0), \quad z_0 = z(0),$$

complement the above equations.

## 4 Resonator feedback field

The Kirchhoff equation (4) can be represented [8, 13] as the integral equation

$$H = -4\pi \int_0^t G(t-t') \dot{m}_x(t') dt', \quad (21)$$

with the transfer function

$$G(t) = \left[ \cos(\bar{\omega}t) - \frac{\gamma}{\bar{\omega}} \sin(\bar{\omega}t) \right] e^{-\gamma t}, \quad \bar{\omega} \equiv \sqrt{\omega^2 - \gamma^2},$$

and where

$$\dot{m}_x = \frac{\mu_0 N S}{2V_c} \frac{d}{dt} (u^* + u). \quad (22)$$

The longitudinal and transverse attenuations are assumed to be small, as compared to the Zeeman frequency,

$$\frac{\gamma_1}{\omega_0} \ll 1, \quad \frac{\gamma_2}{\omega_0} \ll 1. \quad (23)$$

The coupling of the magnet with the resonant electric circuit leads to the appearance of the *coupling attenuation*

$$\gamma_c \equiv \pi \mu_0^2 S \frac{N}{V_c}. \quad (24)$$

The latter, together with the circuit attenuation, are small, as compared to the resonator natural frequency,

$$\frac{\gamma}{\omega} \ll 1, \quad \frac{\gamma_c}{\omega} \ll 1. \quad (25)$$

The stochastic variables (16), because of condition (15), can also be treated as effectively small.

To be efficient, the resonator has to be tuned to the Zeeman frequency, so that the resonance condition

$$\frac{|\Delta|}{\omega} \ll 1 \quad (\Delta \equiv \omega - \omega_0) \quad (26)$$

be valid. Also, the magnetic anisotropy has to be small, with the anisotropy parameter

$$A \equiv \frac{S \Delta J}{\omega_0} < 1. \quad (27)$$

Otherwise the sample magnetization would be frozen.

In this way, the feedback equation (21) can be solved iteratively, taking for the initial approximation  $u \approx u_0 \exp(-i\omega_S t)$ , with

$$\omega_S \equiv \omega_0 - S\Delta Jz = \omega_0(1 - Az) . \quad (28)$$

Then in the first iteration, we get

$$\mu_0 H = i(u\psi - u^*\psi^*) , \quad (29)$$

with the coupling function

$$\psi = \gamma_c \omega_S \left[ \frac{1 - \exp\{-i(\omega - \omega_S)t - \gamma t\}}{\gamma + i(\omega - \omega_S)} + \frac{1 - \exp\{-i(\omega + \omega_S)t - \gamma t\}}{\gamma - i(\omega + \omega_S)} \right] . \quad (30)$$

In view of the above conditions, the first, resonant, term of the coupling function prevails, so that

$$\psi \cong \gamma_c \omega_S \frac{1 - \exp\{-i\Delta_S t - \gamma t\}}{\gamma + i\Delta_S} , \quad (31)$$

with the effective dynamic detuning

$$\Delta_S \equiv \omega - \omega_S = \Delta + \omega_0 A z . \quad (32)$$

Defining the dimensionless coupling parameter

$$g \equiv \frac{\gamma_c \omega_0}{\gamma \gamma_2} , \quad (33)$$

the real and imaginary parts of the coupling function can be written as

$$\text{Re}\psi = g \frac{\gamma^2 \gamma_2}{\gamma^2 + \Delta_S^2} (1 - Az) \left\{ 1 - \left[ \cos(\Delta_S t) - \frac{\Delta_S}{\gamma} \sin(\Delta_S t) \right] e^{-\gamma t} \right\} \quad (34)$$

and, respectively,

$$\text{Im}\psi = -g \frac{\gamma \gamma_2 \Delta_S}{\gamma^2 + \Delta_S^2} (1 - Az) \left\{ 1 - \left[ \cos(\Delta_S t) + \frac{\gamma}{\Delta_S} \sin(\Delta_S t) \right] e^{-\gamma t} \right\} . \quad (35)$$

Note that in the case of resonance, when  $\Delta = 0$ , and under weak anisotropy  $A \ll 1$ , we have  $\Delta_S \rightarrow 0$ . Then the imaginary part (35) is close to zero, and the real part can be simplified to

$$\text{Re}\psi \approx g \gamma_2 (1 - Az) (1 - e^{-\gamma t}) .$$

The latter form can be employed only when the anisotropy is not strong, so that  $A \ll 1$ .

## 5 Scale separation approach

Substituting equality (28) into the evolution equations (18), (19), and (20), we have the equations for the transverse function,

$$\frac{du}{dt} = -i(\omega_S + \xi_0)u - (\gamma_2 - z\psi)u - z\psi^*u^* + i\xi z , \quad (36)$$

the coherence intensity,

$$\frac{dw}{dt} = -2(\gamma_2 - \alpha z)w + i(u^* \xi - \xi^* u)z - z[\psi u^2 + \psi^*(u^*)^2] , \quad (37)$$

and for the spin polarization,

$$\frac{dz}{dt} = -\alpha w - \frac{i}{2}(u^* \varphi - \varphi^* u) + \frac{1}{2}[\psi u^2 + \psi^*(u^*)^2] - \gamma_1(z - \zeta) . \quad (38)$$

Here the notation

$$\alpha \equiv \frac{1}{2}(\psi^* + \psi) = \text{Re}\psi \quad (39)$$

is introduced.

We solve the system of equations (36), (37), and (38) by resorting to the scale separation approach [6,8,9,13,18,19]. The function  $u$  is classified as fast, while  $w$  and  $z$ , as slow. First, we solve equation (36) for the fast variable, keeping the slow variables as quasi-integrals of motion and taking account of the resonance condition (26). This gives

$$\begin{aligned} u = & u_0 \exp \left\{ -(i\omega_S + \gamma_2 - z\psi)t - i \int_0^t \xi_0(t') dt' \right\} + \\ & + iz \int_0^t \xi(t') \exp \left\{ -(i\omega_S + \gamma_2 - z\psi)(t - t') - i \int_{t'}^t \xi(t'') dt'' \right\} dt' . \end{aligned} \quad (40)$$

Stochastic variables, in view of condition (15), are zero-centered,

$$\langle\langle \xi_0(t) \rangle\rangle = \langle\langle \xi(t) \rangle\rangle = \langle\langle \varphi(t) \rangle\rangle = 0 . \quad (41)$$

The stochastic variable  $\xi_0$  is real, while  $\xi$  and  $\varphi$  are complex-valued. Therefore

$$\langle\langle \xi_0(t)\xi(t') \rangle\rangle = \langle\langle \xi_0(t)\varphi(t') \rangle\rangle = \langle\langle \xi(t)\varphi(t') \rangle\rangle = 0 . \quad (42)$$

For the non-zero pair stochastic correlators, we set

$$\langle\langle \xi^*(t)\xi(t') \rangle\rangle = 2\gamma_3\delta(t - t') , \quad \langle\langle \xi^*(t)\varphi(t') \rangle\rangle = 2\gamma_3\delta(t - t') , \quad (43)$$

with  $\gamma_3$  playing the role of an attenuation caused by stochastic fluctuations.

Substituting expression (40) into equations (37) and (38) and averaging the latter over fast temporal oscillations and stochastic variables, we come to the equations for the guiding centers, describing the coherence intensity,

$$\frac{dw}{dt} = -2(\gamma_2 - \alpha z)w + 2\gamma_3 z^2 \quad (44)$$

and the spin polarization,

$$\frac{dz}{dt} = -\alpha w - \gamma_3 z - \gamma_1(z - \zeta) . \quad (45)$$

Recall that  $\alpha$  is given by equations (34) and (39).

## 6 Triggering spin waves

Stochastic variables are the fluctuations that trigger spin motion. To clarify the nature of stochastic variables, let us show that these correspond to spin waves describing spin fluctuations around the average local spin polarization  $z = z(t)$ . It is worth recalling that spin waves can be well defined for nonequilibrium systems [20, 21].

Spin fluctuations are defined as small oscillations around the average spin, which can be represented as

$$S_j^\alpha = \langle S_j^\alpha \rangle + \delta S_j^\alpha . \quad (46)$$

Substituting this into the equations of motion (9) and (10), we omit, for simplicity, the attenuations, keeping in mind the initial stage of the process, when time is yet much shorter than the relaxation times. Separating the zero-order equations, we get

$$\frac{d}{dt} \langle S_j^- \rangle = -i\omega_S \langle S_j^- \rangle , \quad \frac{d}{dt} \langle S_j^z \rangle = 0 . \quad (47)$$

And to first order, we have

$$\begin{aligned} \frac{d}{dt} \delta S_j^- &= -i (\omega_0 \delta S_j^- + \langle S_j^- \rangle \xi_0 - \langle S_j^z \rangle \xi) , \\ \frac{d}{dt} \delta S_j^z &= \frac{i}{2} (\langle S_j^- \rangle \varphi^* - \langle S_j^+ \rangle \varphi) . \end{aligned} \quad (48)$$

Keeping in mind that  $z$  is a slow variable, from equations (47), we find

$$\langle S_j^- \rangle = u_0 S e^{-i\omega_S t} , \quad \langle S_j^z \rangle = z S . \quad (49)$$

In order to stress the role of fluctuations, let us set  $u_0 = 0$ . Then

$$\delta S_j^- = S_j^- , \quad \delta S_j^z = 0 \quad (u_0 = 0) , \quad (50)$$

where we take into account condition (15). The first of equations (48) yields

$$\frac{d}{dt} S_j^- = -i\omega_0 S_j^- + iz S \xi . \quad (51)$$

Let us employ the Fourier transformation for the ladder spin operators,

$$S_j^- = \sum_k S_k^- e^{i\mathbf{k}\cdot\mathbf{r}_j} , \quad S_k^- = \frac{1}{N} \sum_j S_j^- e^{-i\mathbf{k}\cdot\mathbf{r}_j} ,$$

and for the exchange interactions,

$$J_{ij} = \frac{1}{N} \sum_k J_k e^{i\mathbf{k}\cdot\mathbf{r}_{ij}} , \quad J_k = \sum_{j(\neq i)} J_{ij} e^{-i\mathbf{k}\cdot\mathbf{r}_{ij}} , \quad (\mathbf{r}_{ij} \equiv \mathbf{r}_i - \mathbf{r}_j)$$

with the similar transformation for  $I_{ij}$ . For the stochastic variable  $\xi$ , we get

$$\xi = \sum_k (I_0 - J_k) S_k^- e^{i\mathbf{k}\cdot\mathbf{r}_j} .$$



Then equation (51) reduces to

$$\frac{d}{dt} S_k^- = -i\omega_k S_k^- , \quad (52)$$

with the spin-wave spectrum

$$\omega_k = \omega_0 + zS(J_k - I_0) . \quad (53)$$

For long waves, when  $k \rightarrow 0$ , we obtain

$$\omega_k \simeq \omega_S - \frac{zS}{2} \sum_{j(\neq i)} J_{ij} (\mathbf{k} \cdot \mathbf{r}_{ij})^2 . \quad (54)$$

This demonstrates that stochastic fluctuations are nothing but spin waves.

For what follows, it is useful to keep in mind the restriction

$$w + z^2 = \left| \frac{1}{NS} \sum_{j=1}^N \langle \mathbf{S}_j \rangle \right|^2 \leq 1 , \quad (55)$$

which is necessary to take into account when setting initial conditions for equations (44) and (45).

## 7 Qualitative classification of regimes

Suppose that the initial state of the magnet is nonequilibrium, such that the external magnetic field is directed along the  $z$ -axis, together with spins. Spin waves trigger spin motion, forcing spins to move, which generates the resonator feedback field acting back on spins and collectivizing their motion. The spins tend to reach an equilibrium state, reversing from positive to negative values. The overall dynamics can be classified onto several qualitatively different stages. Below, we give this qualitative classification, setting for simplicity zero detuning  $\Delta = 0$  and considering the limit of negligibly weak anisotropy  $A \rightarrow 0$ . Thus, we set

$$\Delta \rightarrow 0 , \quad A \rightarrow 0 , \quad \Delta_S \rightarrow 0 . \quad (56)$$

Then the coupling function (39) reduces to the simple form

$$\alpha \rightarrow g\gamma_2 (1 - e^{-\gamma t}) . \quad (57)$$

### 7.1 Chaotic stage

At the beginning, before coherence in spin motion sets up at time  $t_{coh}$ , the process is yet chaotic. At short times in the interval

$$0 < t < t_{coh} , \quad (58)$$

the coupling function is yet very small, such that

$$\alpha \ll \gamma_2 , \quad \alpha \ll \gamma_3 . \quad (59)$$

Then the linear in time solutions of equations (44) and (45) are

$$w \simeq w_0 + 2(\gamma_3 z_0^2 - \gamma_2 w_0) t , \quad z \simeq z_0 - [(z_0 - \zeta)\gamma_1 + \gamma_3 z_0] t . \quad (60)$$

This regime lasts till the time, when the coupling function grows, so that

$$\alpha z = \gamma_2 \quad (t = t_{coh}), \quad (61)$$

which defines the *coherence time*

$$t_{coh} = \frac{1}{\gamma} \ln \frac{gz_0}{gz_0 - 1}. \quad (62)$$

At large coupling parameter, this gives

$$t_{coh} = \frac{\gamma_2}{\gamma_c \omega_0 z_0} \quad (gz_0 \gg 1). \quad (63)$$

## 7.2 Coherent stage

After the coherence time, spins become well correlated by means of the resonator feedback field. In the time interval

$$t_{coh} < t < T_2, \quad (64)$$

where  $T_2 \equiv 1/\gamma_2$ , the coupling function is large,

$$\alpha \gg \gamma_1, \quad \alpha \gg \gamma_3, \quad (65)$$

reaching the value

$$\alpha \simeq g\gamma_2 \quad (\gamma_2 < \gamma). \quad (66)$$

The spin-lattice attenuation is usually small, such that  $\gamma_1 \ll \gamma_2$  and  $\gamma_1 \ll \gamma_3$ . Then equations (44) and (45) read as

$$\frac{dw}{dt} = -2\gamma_2(1 - gz)w, \quad \frac{dz}{dt} = -g\gamma_2 w. \quad (67)$$

The exact solutions of these equations give the coherence intensity

$$w = \left( \frac{\gamma_p}{g\gamma_2} \right)^2 \operatorname{sech}^2 \left( \frac{t - t_0}{\tau_p} \right) \quad (68)$$

and the spin polarization

$$z = - \frac{\gamma_p}{g\gamma_2} \tanh \left( \frac{t - t_0}{\tau_p} \right) + \frac{1}{g}. \quad (69)$$

Here  $t_0$  and  $\tau_p$  are the integration constants that are defined by the values  $w(t_{coh}) \equiv w_{coh}$  and  $z(t_{coh}) \equiv z_{coh}$ . This gives the *delay time*

$$t_0 = t_{coh} + \frac{\tau_p}{2} \ln \left| \frac{\gamma_p + \gamma_g}{\gamma_p - \gamma_g} \right| \quad (70)$$

and the *pulse time*

$$\tau_p = \frac{1}{\gamma_p}, \quad (71)$$

where

$$2\gamma_p^2 = \gamma_g^2 \left[ 1 + \sqrt{1 + 4 \left( \frac{g\gamma_2}{\gamma_g} \right)^2 w_{coh}} \right], \quad \gamma_p = \gamma_2 (gz_{coh} - 1). \quad (72)$$

Under a large coupling parameter and small coherence intensity, at the coherence time  $t_{coh}$ , we get

$$\begin{aligned}\gamma_g &\simeq g\gamma_2 z_{coh} & (gz_{coh} \gg 1), \\ \gamma_p &\simeq g\gamma_2 \sqrt{z_{coh}^2 + w_{coh}} & (w_{coh} \ll z_{coh}).\end{aligned}\quad (73)$$

The maximum of the coherence intensity occurs at the time  $t_0$ , being

$$w(t_0) = w_{coh} + \left(z_{coh} - \frac{1}{g}\right)^2. \quad (74)$$

At this moment of time, the spin polarization is

$$z(t_0) = \frac{1}{g}. \quad (75)$$

### 7.3 Relaxation stage

After the transverse decoherence time  $T_2$ , there is the relaxation stage in the interval

$$T_2 < t < T_1, \quad (76)$$

where  $T_1 \equiv 1/\gamma_1$ . For  $t \gg t_0$ , the coherence intensity relaxes as

$$w \simeq 4w(t_0) \exp\left(-\frac{2t}{\tau_p}\right), \quad (77)$$

and the spin polarization tends to

$$z \simeq -z_{coh} + \frac{2}{g} + 2\left(z_{coh} - \frac{1}{g}\right) \exp\left(-\frac{2t}{\tau_p}\right). \quad (78)$$

### 7.4 Quasi-stationary stage

In the limit of very long times, when

$$T_1 < t < \infty, \quad (79)$$

the solutions exhibit small oscillations around the fixed points  $w^*$  and  $z^*$  given by the equations

$$\gamma_2(1 - gz^*)w^* - \gamma_3(z^*)^2 = 0, \quad g\gamma_2 w^* + \gamma_3 z^* + \gamma_1(z^* - \zeta) = 0. \quad (80)$$

### 7.5 Punctuated superradiance

The coherent stage of radiation corresponds to the regime of superradiance, which can be pure, if  $w_0 = 0$ , or triggered, if  $w_0 > 0$ . It is also possible to realize the regime of punctuated superradiance [18], when in the process of spin dynamics either the external magnetic field is reversed or the magnetic sample is rotated, so that to reproduce the initial nonequilibrium conditions. In this case, radiation exhibits a series of coherent pulses, with the temporal intervals that can be regulated.

## 8 Numerical investigation of dynamics

We solve equations (44) and (45) numerically, with the coupling function defined in equations (34) and (39). The case of exact resonance is assumed, with  $\omega = \omega_0$ . Then  $\Delta = 0$  and  $\Delta_S = \omega Az$ . The chosen initial conditions correspond to a purely self-organized process, in the absence of imposed initial coherence, so that  $w_0 = 0$ , and when the initial polarization  $z_0 = 1$  defines a strongly nonequilibrium state, since the equilibrium polarization of a single spin, under the given setup, corresponds to  $\zeta = -1$ .

In the presence of a resonator feedback field, spin reversal happens much faster than the homogeneous transverse relaxation time  $T_2 \equiv 1/\gamma_2$ . We measure all attenuations and frequencies in units of  $\gamma_2$ . The spin-lattice attenuation  $\gamma_1$  is usually much smaller than  $\gamma_2$ . Taking this into account, we set  $\gamma_1 = 0.001$ . The dynamic attenuation  $\gamma_3$  is assumed to be of order of  $\gamma_2$ , which, in units of the latter, implies  $\gamma_3 = 1$ . Time is measured in units of  $T_2$ .

First, we consider the more general form corresponding to expression (34), which reads as

$$\alpha = g \frac{\gamma^2 \gamma_2 (1 - Az)}{\gamma^2 + (\omega Az)^2} \left\{ 1 - \left[ \cos(\omega Az t) - \frac{\omega}{\gamma} Az \sin(\omega Az t) \right] e^{-\gamma t} \right\} .$$

The temporal behaviour of the coherence intensity and spin polarization, for different system parameters, is shown in Figures 1 to 8.

Figures 1 and 2 show the role of magnetic anisotropy for different resonator frequencies. Increasing the anisotropy, generally, shifts the delay time, widens the coherence pulse, and decreases the coherence peak maximum, and the reversed spin polarization.

Figures 3 and 4 demonstrate the role of the resonator attenuation. The larger  $\gamma$ , the higher the coherence peak maximum and the shorter the delay time. Spin reversal is better pronounced for larger attenuations.

Figures 5 and 6 illustrate the role of the coupling strength between the magnet and resonator. The larger coupling parameter leads to a shorter delay time and higher coherence maximum. The value of  $\omega$  does not influence much the behavior, when the anisotropy is weak,  $A \ll 1$ . Stronger coupling leads to a better spin reversal.

Figures 7 and 8 show the role of anisotropy for a large value of the coupling parameter. The stronger anisotropy increases the delay time and diminishes the coherence peak maximum. Spin reversal is more effective for a weaker anisotropy.

The general form of the above coupling function looks a bit cumbersome, because of which we also check its approximate form, discussed in Section 4, which is given by the expression

$$\alpha \approx g \gamma_2 (1 - Az) (1 - e^{-\gamma t}) .$$

It turns out that this approximate form is applicable under weak anisotropy, with the anisotropy parameters  $A \ll 1$ , but becomes invalid for larger anisotropies.

## 9 Spatial distribution of radiation

The spatial distribution of radiation for atomic systems can be found in references [22,23]. In the case of spin systems, the calculational procedure is similar, with the difference that the radiation is produced by moving magnetic moments. The other slight difference is connected with the chosen geometry. For atomic systems, one usually considers a cylindric sample, with the axis along the  $z$  axis. In the setup, related to a magnetic system, as we study here, the

magnetic sample is inserted into a coil, with the axis along the  $x$  axis, while an external magnetic field defines the  $z$  axis, so that the sample axis is orthogonal to the  $z$  axis.

The operator of magnetic moment, related to a  $j$ -th spin, can be written in the form

$$\mu_0 \mathbf{S}_j = \vec{\mu} S_j^+ + \vec{\mu}^* S_j^- + \vec{\mu}_0 S_j^z, \quad (81)$$

where

$$\vec{\mu} = \frac{\mu_0}{2} (\mathbf{e}_x - i\mathbf{e}_y), \quad \vec{\mu}_0 = \mu_0 \mathbf{e}_z. \quad (82)$$

The radiation intensity in the direction of the vector

$$\mathbf{n} \equiv \frac{\mathbf{r}}{|\mathbf{r}|} = \frac{\mathbf{r}}{r} \quad (83)$$

can be represented [19] as

$$I(\mathbf{n}, t) = 2\omega_0 \gamma_0 \sum_{ij} \varphi_{ij}(\mathbf{n}) \langle S_i^+(t) S_j^-(t) \rangle, \quad (84)$$

where  $\gamma_0$  is a natural width,

$$\gamma_0 \equiv \frac{2}{3} |\vec{\mu}|^2 k_0^3 = \frac{1}{3} \mu_0^2 k_0^3 \quad \left( k_0 \equiv \frac{\omega_0}{c} \right), \quad (85)$$

and the system form-factor is

$$\varphi_{ij}(\mathbf{n}) = \frac{3}{8\pi} |\mathbf{n} \times \mathbf{e}_\mu|^2 \exp(ik_0 \mathbf{n} \cdot \mathbf{r}_{ij}). \quad (86)$$

Here we introduce the unit vector

$$\mathbf{e}_\mu \equiv \frac{\vec{\mu}}{|\vec{\mu}|} = \frac{1}{\sqrt{2}} (\mathbf{e}_x - i\mathbf{e}_y) \quad (87)$$

and take into account that

$$|\vec{\mu}| = \frac{\mu_0^2}{2}, \quad |\vec{\mu}_0|^2 = \mu_0^2.$$

Denoting by  $\vartheta$  the angle between  $\mathbf{n}$  and  $\mathbf{e}_\mu$ , we have

$$|\mathbf{n} \times \mathbf{e}_\mu|^2 = 1 - \frac{1}{2} \sin^2 \vartheta = \frac{1}{2} (1 + \cos^2 \vartheta).$$

The form factor (86) becomes

$$\varphi_{ij}(\mathbf{n}) = \frac{3}{16\pi} (1 + \cos^2 \vartheta) \exp(ik_0 \mathbf{n} \cdot \mathbf{r}_{ij}). \quad (88)$$

The radiation intensity (84) can be separated into two terms,

$$I(\mathbf{n}, t) = I_{inc}(\mathbf{n}, t) + I_{coh}(\mathbf{n}, t), \quad (89)$$

the incoherent radiation intensity

$$I_{inc}(\mathbf{n}, t) = 2\omega_0 \gamma_0 \sum_j \varphi(\mathbf{n}) \langle S_j^+(t) S_j^-(t) \rangle, \quad (90)$$

and the coherent radiation intensity

$$I_{coh}(\mathbf{n}, t) = 2\omega_0\gamma_0 \sum_{i \neq j} \varphi_{ij}(\mathbf{n}) \langle S_i^+(t) S_j^-(t) \rangle , \quad (91)$$

where

$$\varphi(\mathbf{n}) \equiv \varphi_{jj}(\mathbf{n}) = \frac{3}{16\pi} (1 + \cos^2 \vartheta) . \quad (92)$$

Taking into account the identity

$$S_j^+ S_j^- = S(S+1) - (S_j^z)^2 + S_j^z$$

and the approximate equality

$$\langle (S_j^z)^2 \rangle \approx S^2 ,$$

which is exact for spin  $S = 1/2$ , as well as for large  $S \rightarrow \infty$ , makes it possible to rewrite the incoherent radiation intensity as

$$I_{inc}(\mathbf{n}, t) = 2\omega_0\gamma_0 \sum_j \varphi(\mathbf{n}) (S + \langle S_j^z \rangle) . \quad (93)$$

Introducing the local functions

$$\begin{aligned} u_j(t) &\equiv \frac{1}{S} \langle S_j^-(t) \rangle , & w_j(t) &\equiv \frac{1}{S^2} | \langle S_j^-(t) \rangle |^2 , \\ z_j(t) &\equiv \frac{1}{S} \langle S_j^z(t) \rangle , \end{aligned} \quad (94)$$

and using the semiclassical approximation, we come to the incoherent radiation intensity

$$I_{inc}(\mathbf{n}, t) = 2\omega_0\gamma_0 S \sum_j \varphi_{ij}(\mathbf{n}) [1 + z_j(t)] , \quad (95)$$

and the coherent radiation intensity

$$I_{coh}(\mathbf{n}, t) = 2\omega_0\gamma_0 S^2 \sum_{i \neq j} \varphi_{ij}(\mathbf{n}) u_i^*(t) u_j(t) . \quad (96)$$

Assuming that the radiation wave length is comparable or larger than the linear sample sizes, we can resort to the uniform approximation, passing to functions (11), (12), and (13). In this procedure, we consider the sum

$$\sum_{i \neq j} \varphi_{ij}(\mathbf{n}) = \varphi(\mathbf{n}) N^2 \left[ F(k_0 \mathbf{n}) - \frac{1}{N^2} \right] , \quad (97)$$

in which

$$F(k_0 \mathbf{n}) \equiv \left| \frac{1}{N} \sum_{j=1}^N e^{ik_0 \mathbf{n} \cdot \mathbf{r}_j} \right|^2 . \quad (98)$$

Then we find the incoherent radiation intensity

$$I_{inc}(\mathbf{n}, t) = 2\omega_0\gamma_0 N S \varphi(\mathbf{n}) [1 + z(t)] \quad (99)$$

and the coherent radiation intensity

$$I_{coh}(\mathbf{n}, t) = 2\omega_0\gamma_0 N^2 S^2 \varphi(\mathbf{n}) F(k_0\mathbf{n}) w(t) . \quad (100)$$

The total radiation intensity, integrated over the spherical angles, is

$$I(t) \equiv \int I(\mathbf{n}, t) d\Omega(\mathbf{n}) = I_{inc}(t) + I_{coh}(t) , \quad (101)$$

containing the incoherent part

$$I_{inc}(t) = 2\omega_0\gamma_0 SN[1 + z(t)] \quad (102)$$

and the coherent part

$$I_{coh}(t) = 2\omega_0\gamma_0 S^2 N^2 \varphi_0 w(t) , \quad (103)$$

with the shape factor

$$\varphi_0 \equiv \int \varphi(\mathbf{n}) F(k_0\mathbf{n}) d\Omega(\mathbf{n}) . \quad (104)$$

When spins are uniformly distributed in the sample, function (98) can be represented as an integral over the sample volume:

$$F(k_0\mathbf{n}) = \left| \frac{1}{V} \int_V e^{ik_0\mathbf{n}\cdot\mathbf{r}} d\mathbf{r} \right|^2 . \quad (105)$$

The direction vector, in terms of spherical coordinates, is

$$\mathbf{n} = \{ \sin \vartheta \cos \varphi, \sin \vartheta \sin \varphi, \cos \vartheta \} . \quad (106)$$

Integrating over the sample, we meet the integral

$$\int_0^a \sin \left( c\sqrt{a^2 - x^2} \right) \cos(bx) dx = \frac{\pi ac}{2\sqrt{b^2 + c^2}} J_1 \left( a\sqrt{b^2 + c^2} \right)$$

expressed through the Bessel function  $J_1$  of the first kind. Finally, we obtain

$$F(k_0\mathbf{n}) = \frac{16 \sin^2 \left( \frac{k_0 L}{2} \sin \vartheta \cos \varphi \right)}{k_0^2 L^2 \sin^2 \vartheta \cos^2 \varphi} \frac{J_1^2 \left( k_0 R \sqrt{\sin^2 \vartheta \sin^2 \varphi + \cos^2 \vartheta} \right)}{k_0^2 R^2 (\sin^2 \vartheta \sin^2 \varphi + \cos^2 \vartheta)} . \quad (107)$$

Recall that  $k_0 \equiv \omega_0/c = 2\pi/\lambda$ .

Since the magnetic sample is inserted into a coil aligned along the axis  $x$ , the radiation in the  $z$  direction is absorbed by the coil. Radiation can be emitted only in the  $x$  direction, when

$$F(k_0\mathbf{n}) = \frac{4}{k_0^2 L^2} \sin^2 \left( \frac{k_0 L}{2} \right) \quad \left( \vartheta = \frac{\pi}{2}, \varphi = 0 \right) . \quad (108)$$

Then  $\varphi(\mathbf{n}) = 3/(16\pi)$ , which is only twice smaller than its value in the  $z$  direction.

If the sample is a very narrow cylinder, or represents a linear chain of spins aligned along the axis  $x$ , then expression (107) leads to

$$F(k_0\mathbf{n}) = \frac{4 \sin^2 \left( \frac{k_0 L}{2} \sin \vartheta \cos \varphi \right)}{k_0^2 L^2 \sin^2 \vartheta \cos^2 \varphi} \quad (R \rightarrow 0) . \quad (109)$$

Magnetic dipole radiation usually corresponds to long waves, such that the wavelength  $\lambda$  is longer than the sample linear sizes. To consider this limit, we notice that the Bessel function  $J_\nu(x)$ , at small  $x \ll 1$ , has the asymptotic property

$$J_\nu(x) \simeq \frac{1}{\Gamma(\nu+1)} \left(\frac{x}{2}\right)^\nu - \frac{1}{\Gamma(\nu+2)} \left(\frac{x}{2}\right)^{\nu+2},$$

because of which

$$J_1(x) \simeq \frac{x}{2} \quad (x \rightarrow 0).$$

Hence, in the long-wave limit,

$$F(k_0 \mathbf{n}) \simeq 1 \quad \left( \frac{2\pi R}{\lambda} \ll 1, \frac{\pi L}{\lambda} \ll 1 \right). \quad (110)$$

In this way, although a part of radiation is absorbed by the coil, nevertheless, an essential part of radiation can be emitted through the sides of the sample along the coil axis  $x$ .

## 10 Discussion

We have considered a large class of magnetic materials, composed of particles interacting through exchange interactions. Such materials are well represented by an anisotropic Heisenberg Hamiltonian. By coupling a magnetic sample to a resonant electric circuit it is possible to efficiently regulate spin dynamics. The present investigation complements the earlier studies of spin dynamics in different materials, accomplished for polarized nuclei, magnetic nanomolecules, and magnetic nanoclusters. The systems composed of these particles possess several common properties. Such systems, except polarized nuclei, exhibit magnetic anisotropy. For example, the spins of magnetic nanomolecules are frozen below the blocking temperature  $T_B \sim 1 - 10$  K, with the frozen magnetization protected by an anisotropy barrier of energy  $E_A \sim 10 - 100$  K. For magnetic nanoclusters, the blocking temperature is  $T_B \sim 10 - 100$  K. Polarized nuclei can be represented by polarized protons in hydrogenated materials, such as propanediol, butanol, and ammonia. Although these materials do not enjoy magnetic anisotropy, however their spins, at low temperature, can remain polarized for extremely long time. The common feature of all above materials is that their spin interactions are described by dipolar forces.

However, there exists a very wide class of materials made of particles with magnetic exchange interactions. Also, recently there have appeared a new type of magnetic nanomaterials characterized by exchange interactions, such as magnetic graphene, where magnetic properties are induced by defects [2–4].

Graphene is a two-dimensional carbon material intermediate between an insulator and a metal [24, 25]. Carbon-carbon spacing is  $a \approx 1.42$  Å, and its surface density is  $\rho \approx 3.9 \times 10^{15}$  cm<sup>-2</sup>.

Magnetic graphene can be well described by an anisotropic Heisenberg model [2–4]. For defects on a zigzag edge, one has an exchange interaction potential  $J \sim 0.1$  eV, or  $J \sim 10^{-13}$  erg. This gives  $J/\hbar \sim 10^{14}$  s<sup>-1</sup> and  $J/k_B \sim 10^3$  K. Dipolar interactions are much weaker, with  $\mu_B^2/a^3 \sim 10^{-17}$  erg, or  $\mu_B^2/(\hbar a^3) \sim 10^{10}$  s<sup>-1</sup>. In temperature units, this gives  $\mu_B^2/(k_B a^3) \sim 0.1$  K. Magnetic anisotropy is not strong, with  $\Delta J/J \sim 10^{-4}$ , hence,  $\Delta J/\hbar \sim 10^{10}$  s<sup>-1</sup>. Thus,  $\gamma_2 \sim \mu_B^2/(\hbar a^3) \sim 10^{10}$  s<sup>-1</sup>. If  $\gamma_3 \sim \Delta J/\hbar$ , then  $\gamma_3 \sim 10^{10}$  s<sup>-1</sup>, that is, of the same



order as  $\gamma_2$ . In the case of an external magnetic field  $B_0 = 1$  T, the Zeeman frequency is  $\omega_0 = |\mu_B B_0|/\hbar \sim 10^{11}$  s $^{-1}$ . Therefore the radiation wavelength is  $\lambda \sim 10$  cm. Since there are many ways of generating defects in graphene, the system parameters can be varied.

It is important to stress that a self-organized spin dynamics, when there is no initial coherence imposed onto the sample, cannot be correctly described by phenomenological equations, like Landau-Lifshitz, Gilbert, or Bloch equations. This is why, we use a microscopic approach with a realistic Hamiltonian. Such an approach makes it possible to take into account quantum fluctuations, crucially important at the beginning of spin relaxation. Also, the use of a microscopic model has an advantage of containing well defined parameters associated with the considered Hamiltonian.

When the system is prepared in a nonequilibrium state, and no initial coherence is imposed onto the sample, spin wave fluctuations serve as a triggering mechanism starting spin motion. It is possible to show that spin wave fluctuations is the sole triggering mechanism, while thermal Nyquist noise of the coil cannot play the role of a trigger.

In the process of motion, spins are collectivized by means of the resonator feedback field. Superradiance in spin systems cannot be caused by photon exchange. That is, spin superradiance is due to the Purcell effect and is impossible without a resonator. This is contrary to atomic systems, where superradiance develops as a Dicke effect.

The microscopic equations of motion are investigated by employing stochastic mean-field approximation and scale separation approach. The equations for guiding centers are solved numerically. Depending on initial conditions and system parameters, there can exist different regimes of spin dynamics, slow free relaxation during the time  $T_1$ , free induction in time  $T_2$ , weak superradiance in time slightly shorter than  $T_2$ , pure superradiance and triggered superradiance, when the reversal time of magnetization can be made much shorter than  $T_2$ , of order  $10^{-11}$  s or  $10^{-12}$  s. The regime of punctuated superradiance can be realized, producing a sequence of coherent pulses.

We have analyzed the spatial distribution of radiation produced by moving magnetic moments. Although a part of radiation is absorbed by the coil surrounding the sample, anyway, radiation can be emitted through the sides of the sample, where there is no coil.

The studied effects can be used in a variety of problems in spintronics and in quantum information processing.

**Acknowledgement.** Financial support from RFBR (grant # 14-02-00723) is appreciated.

## References

- [1] Evans RFL, Fan WJ, Chureemart P, Ostler TA, Ellis MOA and Chantrell RW 2014 *J. Phys. Condens. Matter* **26** 103202
- [2] Yaziev OV 2010 *Rep Prog Phys* **73** 056501
- [3] Katsnelson MI 2012 *Graphene: Carbon in Two Dimensions* (Cambridge: Cambridge University Press)
- [4] Enoki T and Ando T 2013 *Physics and Chemistry of Graphene* (Singapore: Pan Stanford)
- [5] Purcell EM 1946 *Phys. Rev.* **69** 681
- [6] Yukalov VI 1995 *Phys. Rev. Lett.* **75** 3000
- [7] Yukalov VI 1995 *Laser Phys.* **5** 526
- [8] Yukalov VI 1995 *Laser Phys.* **5** 970
- [9] Yukalov VI 1996 *Phys. Rev. B* **53** 9232
- [10] Yukalov VI, Yukalova EP 1998 *Laser Phys.* **8** 1029
- [11] Yukalov VI 2002 *Laser Phys.* **12** 1089
- [12] Yukalov VI, Yukalova EP 2005 *Eur. Phys. Lett.* **70** 306
- [13] Yukalov VI 2005 *Phys. Rev. B* **71** 184432
- [14] Yukalov VI, Henner VK, Kharebov PV, Yukalova EP 2008 *Laser Phys. Lett.* **5** 887
- [15] Yukalov VI, Yukalova EP 2011 *Laser Phys. Lett.* **8** 804
- [16] Yukalov VI, Yukalova EP 2012 *J. Appl. Phys.* **111** 023911
- [17] Kharebov PV, Henner VK, Yukalov VI 2013 *J. Appl. Phys.* **113** 043902
- [18] Yukalov VI, Yukalova EP 2004 *Phys. Part. Nucl.* **35** 348
- [19] Yukalov VI 2014 *Laser Phys.* **24** 094015
- [20] Rückriegel A, Kreisel A, Kopietz P 2012 *Phys. Rev. B* **85** 054422
- [21] Birman JL, Nazmitdinov RG, Yukalov VI 2013 *Phys. Rep* **526** 1
- [22] Rehler NE, Eberly JH 1971 *Phys. Rev. A* **3** 1735
- [23] Allen L, Eberly JH 1975 *Optical Resonance and Two-Level Atoms* (New York: Wiley)
- [24] Goerbig MO 2011 *Rev. Mod. Phys.* **83** 1193
- [25] Wehling TO, Black-Schaffer AM, Balatsky AV 2014 *Adv. Phys.* **63** 1

## Figure Captions

**Figure 1.** Role of magnetic anisotropy in spin dynamics for the parameters  $\gamma = 1$ ,  $g = 10$ , and  $\omega = 10$ , under different anisotropy parameters,  $A = 0.1$  (solid line),  $A = 0.5$  (dashed line), and  $A = 1$  (dashed-dotted line): (a) Coherence intensity; (b) Spin polarization.

**Figure 2.** Role of magnetic anisotropy in spin dynamics for the parameters  $\gamma = 1$ ,  $g = 10$ , but  $\omega = 100$ , under different anisotropy parameters,  $A = 0.1$  (solid line),  $A = 0.5$  (dashed line), and  $A = 1$  (dashed-dotted line): (a) Coherence intensity; (b) Spin polarization.

**Figure 3.** Role of resonator attenuation for the parameters  $g = 10$ ,  $A = 0.1$ , and  $\omega = 10$ , under different attenuation parameters,  $\gamma = 1$  (solid line),  $\gamma = 10$  (dashed line), and  $\gamma = 100$  (dashed-dotted line): (a) Coherence intensity; (b) Spin polarization.

**Figure 4.** Role of resonator attenuation for the parameters  $g = 10$ ,  $A = 0.1$ , but  $\omega = 100$ , under different attenuation parameters,  $\gamma = 1$  (solid line),  $\gamma = 10$  (dashed line), and  $\gamma = 100$  (dashed-dotted line): (a) Coherence intensity; (b) Spin polarization.

**Figure 5.** Role of magnet-resonator coupling for the parameters  $\gamma = 10$ ,  $A = 0.1$ , and  $\omega = 10$ , under different coupling parameters  $g = 10$  (solid line) and  $g = 100$  (dashed line): (a) Coherence intensity; (b) Spin polarization.

**Figure 6.** Role of magnet-resonator coupling for the parameters  $\gamma = 10$ ,  $A = 0.1$ , but  $\omega = 100$ , under different coupling parameters,  $g = 10$  (solid line) and  $g = 100$  (dashed line): (a) Coherence intensity; (b) Spin polarization.

**Figure 7.** Role of magnetic anisotropy for the parameters  $\gamma = 10$ ,  $g = 100$ , and  $\omega = 10$ , under different anisotropy parameters,  $A = 0$  (solid line),  $A = 0.1$  (dashed line),  $A = 0.5$  (dashed-dotted line), and  $A = 1$  (dashed line with dots): (a) Coherence intensity; (b) Spin polarization.

**Figure 8.** Role of magnetic anisotropy for the parameters  $\gamma = 10$ ,  $g = 100$ , but  $\omega = 100$ , under different anisotropy parameters,  $A = 0$  (solid line),  $A = 0.1$  (dashed line),  $A = 0.5$  (dashed-dotted line), and  $A = 1$  (dotted line): (a) Coherence intensity; (b) Spin polarization.

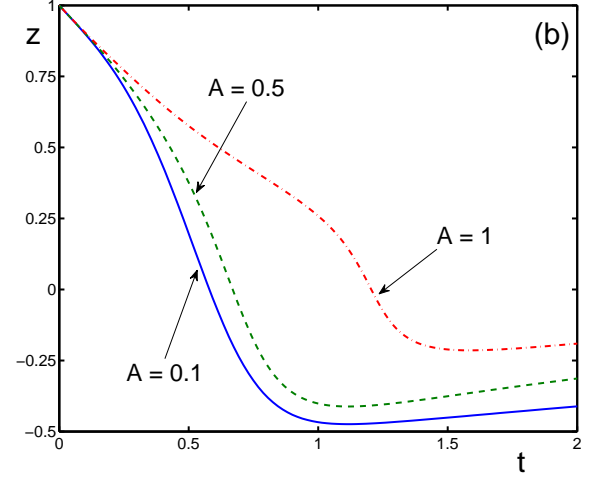
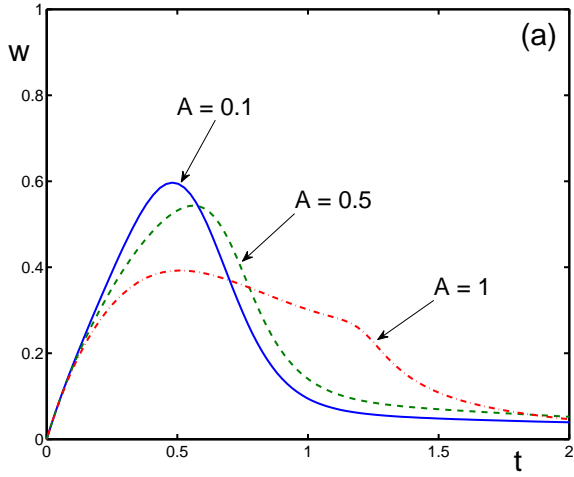


Figure 1: Role of magnetic anisotropy in spin dynamics for the parameters  $\gamma = 1$ ,  $g = 10$ , and  $\omega = 10$ , under different anisotropy parameters,  $A = 0.1$  (solid line),  $A = 0.5$  (dashed line), and  $A = 1$  (dashed-dotted line): (a) Coherence intensity; (b) Spin polarization.

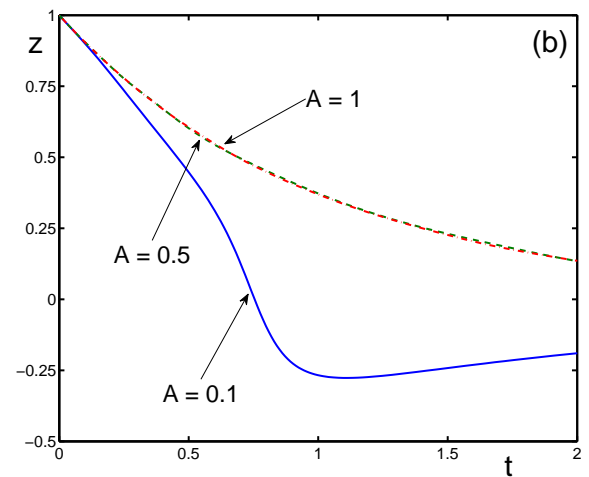
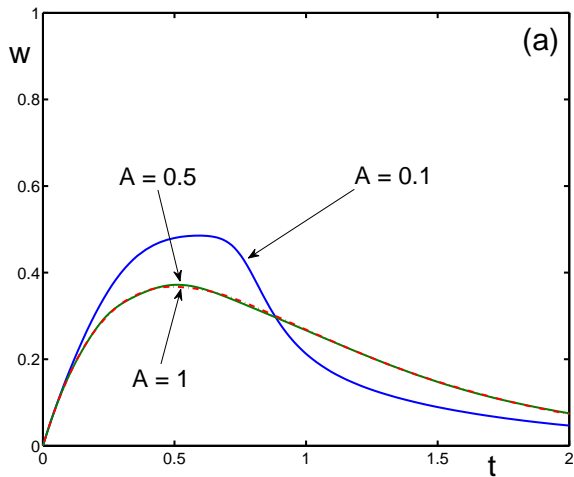


Figure 2: Role of magnetic anisotropy in spin dynamics for the parameters  $\gamma = 1$ ,  $g = 10$ , but  $\omega = 100$ , under different anisotropy parameters,  $A = 0.1$  (solid line),  $A = 0.5$  (dashed line), and  $A = 1$  (dashed-dotted line): (a) Coherence intensity; (b) Spin polarization.

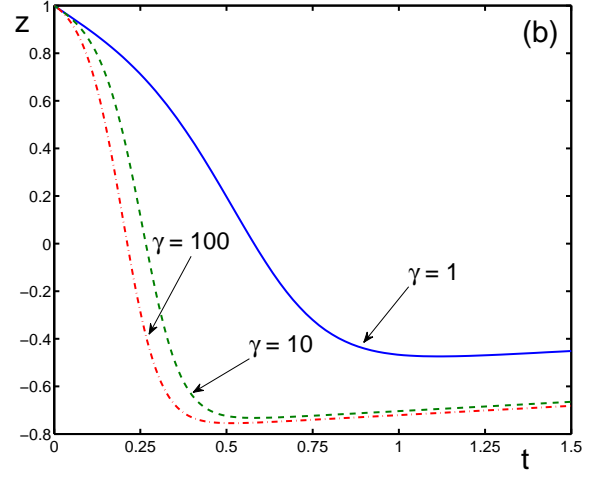
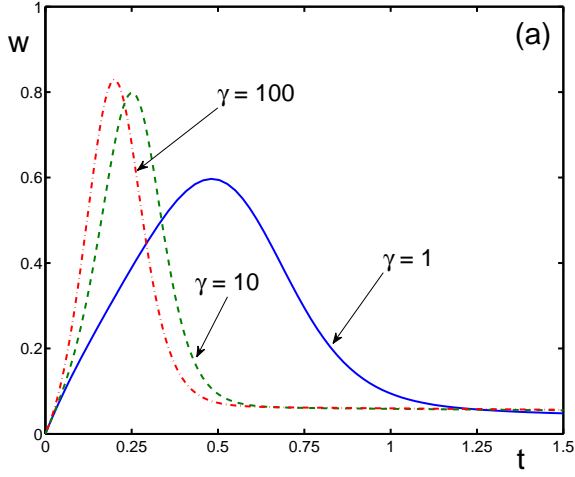


Figure 3: Role of resonator attenuation for the parameters  $g = 10$ ,  $A = 0.1$ , and  $\omega = 10$ , under different attenuation parameters,  $\gamma = 1$  (solid line),  $\gamma = 10$  (dashed line), and  $\gamma = 100$  (dashed-dotted line): (a) Coherence intensity; (b) Spin polarization.

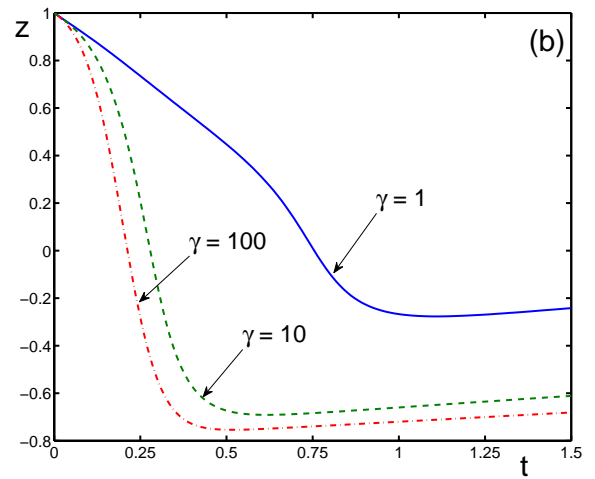
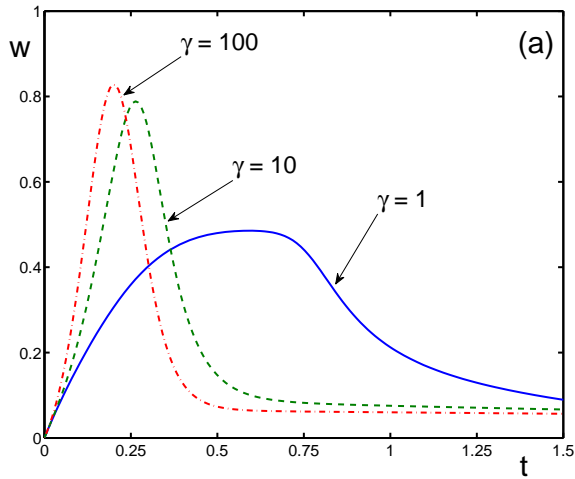


Figure 4: Role of resonator attenuation for the parameters  $g = 10$ ,  $A = 0.1$ , but  $\omega = 100$ , under different attenuation parameters,  $\gamma = 1$  (solid line),  $\gamma = 10$  (dashed line), and  $\gamma = 100$  (dashed-dotted line): (a) Coherence intensity; (b) Spin polarization.

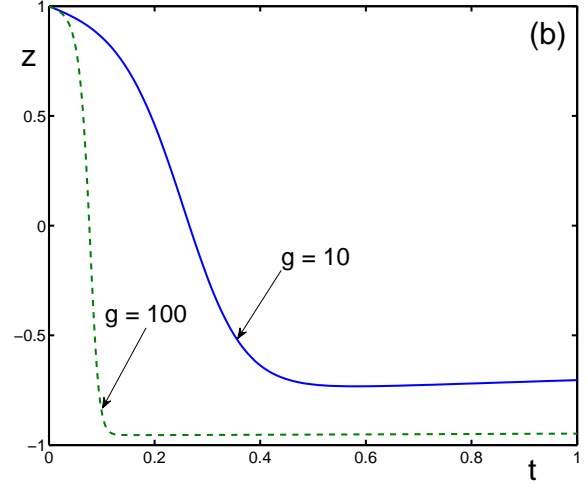
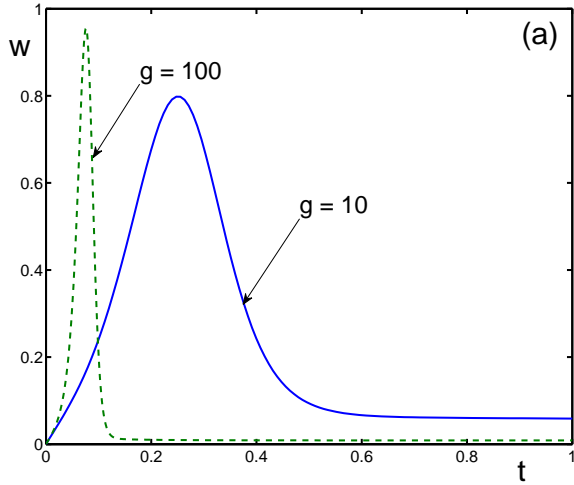


Figure 5: Role of magnet-resonator coupling for the parameters  $\gamma = 10$ ,  $A = 0.1$ , and  $\omega = 10$ , under different coupling parameters  $g = 10$  (solid line) and  $g = 100$  (dashed line): (a) Coherence intensity; (b) Spin polarization.

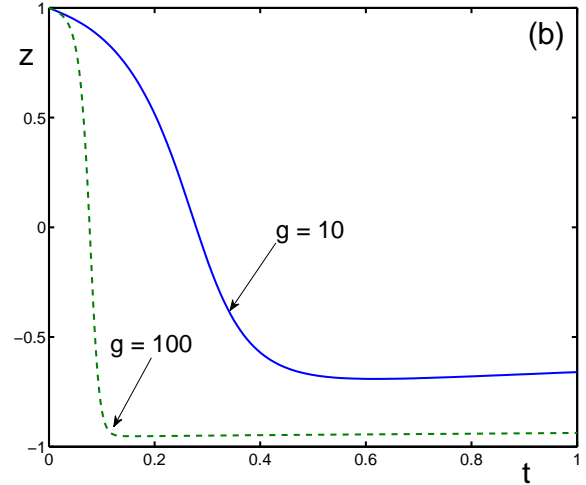
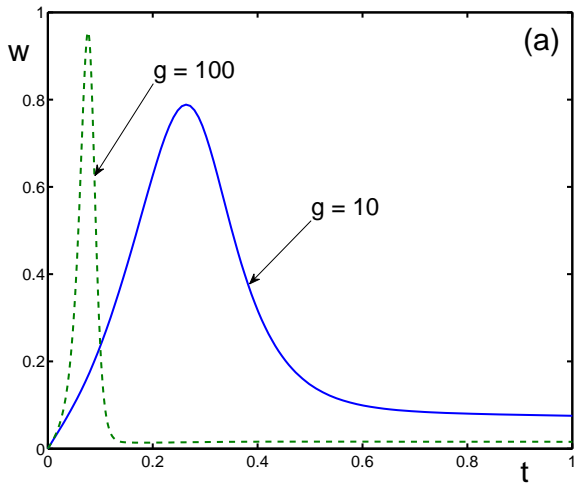


Figure 6: Role of magnet-resonator coupling for the parameters  $\gamma = 10$ ,  $A = 0.1$ , but  $\omega = 100$ , under different coupling parameters,  $g = 10$  (solid line) and  $g = 100$  (dashed line): (a) Coherence intensity; (b) Spin polarization.

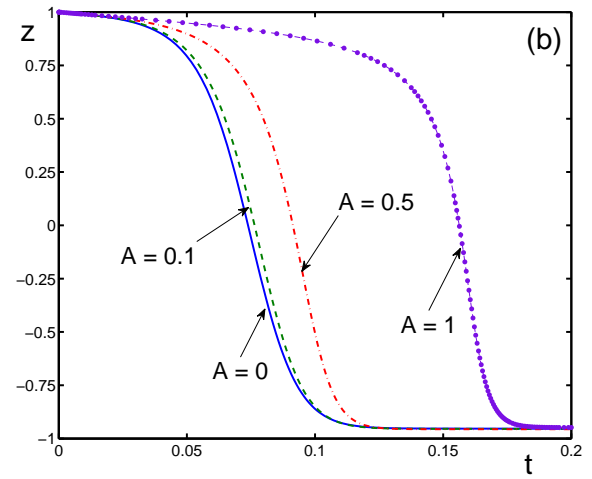
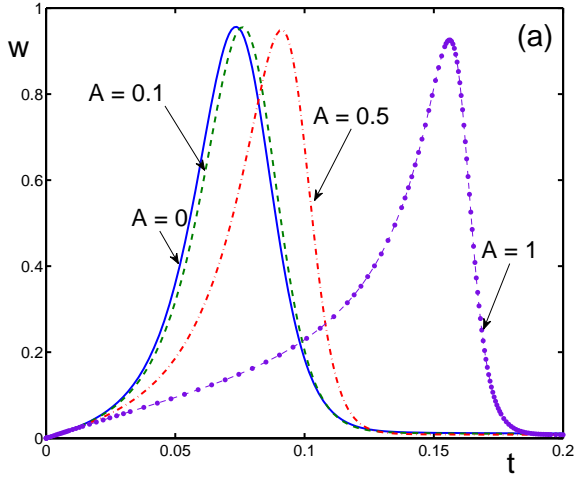


Figure 7: Role of magnetic anisotropy for the parameters  $\gamma = 10$ ,  $g = 100$ , and  $\omega = 10$ , under different anisotropy parameters,  $A = 0$  (solid line),  $A = 0.1$  (dashed line),  $A = 0.5$  (dashed-dotted line), and  $A = 1$  (dashed line with dots): (a) Coherence intensity; (b) Spin polarization.

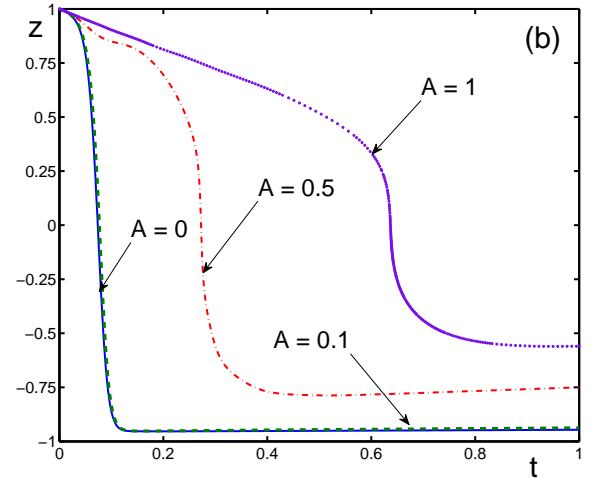
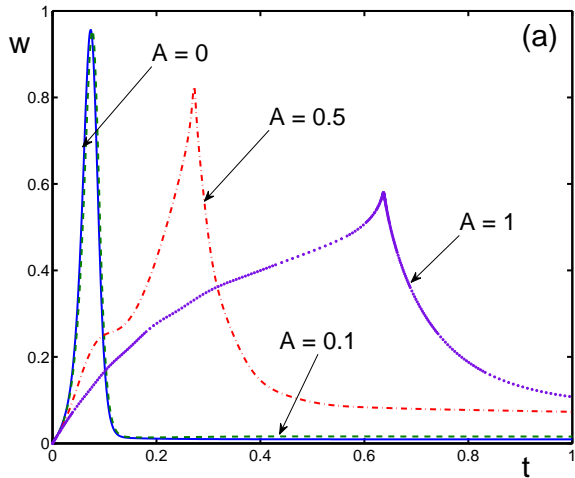


Figure 8: Role of magnetic anisotropy for the parameters  $\gamma = 10$ ,  $g = 100$ , but  $\omega = 100$ , under different anisotropy parameters,  $A = 0$  (solid line),  $A = 0.1$  (dashed line),  $A = 0.5$  (dashed-dotted line), and  $A = 1$  (dotted line): (a) Coherence intensity; (b) Spin polarization.